Composite Structures 344 (2024) 118318

Contents lists available at ScienceDirect

Composite Structures

journal homepage: www.elsevier.com/locate/compstruct

Low-Velocity Impact of carbon, flax, and hybrid composites: Performance comparison and numerical modeling

Giulia Del Bianco [a], Valentina Giammaria [a], Monica Capretti [a], Simonetta Boria [a], Stefano Lenci [b,*], Raffaele Ciardiello [c], Vincenzo Castorani [d]

[a] School of Sciences and Technology, Mathematics division, University of Camerino, Via Madonna delle Carceri 9, 62032 Camerino, Italy
[b] Department of Civil Engineering, Construction and Architecture, Polytechnic University of Marche, Via Brecce Bianche, 60131 Ancona, Italy
[c] Department of Mechanical and Aerospace Engineering, Polytechnic University of Turin, Corso Duca degli Abruzzi 24, 10129 Torino, Italy
[d] HP Composites SpA, Department of Research & Development, Via del Lampo S.N., Z.Ind.le Campolungo, 63100 Ascoli Piceno, Italy

ARTICLE INFO

Keywords:
Natural fibers
Toughened epoxy resin
Hybrid composites
Impact behavior
Finite element analysis
LS-DYNA
Energy absorbers

ABSTRACT

In recent years, composite materials have assumed an increasingly dominant role in various industrial sectors, combining lightweight with optimal mechanical properties. In this context, natural fibers are essential for the development of eco-friendly composites, ensuring a balance between performance and sustainability via hybridization. This study provides an experimental and numerical analysis on composite laminates subjected to Low-Velocity Impact (LVI) tests at different energy levels, after an initial mechanical characterization of the materials. Carbon and flax fiber fabrics are chosen as reinforcements embedded in a toughened epoxy resin, as well as in two hybrid configurations; two different stacking sequences are also investigated, with the layers placed at 0° and in a quasi-isotropic (ISO) orientation. Hysteresis curves and energy absorption capability – in terms of specific energy absorption (SEA) – are then discussed and compared to each other, along with cross-shaped damage propagation on fracture surfaces. Numerical finite element (FE) models of tensile, compressive, and LVI tests are designed and solved using LS-DYNA software. In particular, tensile and compressive ones are carried out to calibrate the material cards, which have subsequently been adopted in the LVI models. The results obtained not only show an agreement between the experimental response and the simulated one, but also provide a complete investigation of different materials and orientations under LVI in view of future applications, highlighting the possibility of designing structural components to absorb energy in hybrid composites reinforced with natural fibers.

1. Introduction

The recent advancements in material science coupled with the growing emphasis on sustainability have led to an in deep interest towards the world of natural fibers and the composites arising from them [1]. Nowadays, natural fibers – such as jute, flax, hemp, sisal, and kenaf [2] – are being combined with a wide range of polymers – typically resins – or other matrices, resulting in Natural Fiber Composites (NFC) [3]. This increasing interest in NFC during the last years denoted a growing awareness of the need for sustainable and bio-based materials in many areas. In order to limit the advance rate of climate change, also the manufacturing processes related to these new green materials are slowly evolving by improving resources management, controlling emissions into the atmosphere, and reducing environmental pollution.

These materials offer a combination of lightweight, biodegradable, and interesting damping properties, all qualities that are useful to create versatile and eco-friendly products in different application fields. In particular, one key advantage of NFC is their low-cost compared to traditional composites made from synthetic fibers, typically carbon ones. Another noteworthy advantage is the short supply chain linked to the production of these materials; since natural fibers are readily available and can be locally sourced, transportation costs and carbon footprint are strongly reduced. Therefore, these composites are promising to re-think product design in a sustainable perspective, associated with related changes in manufacturing techniques. In this context, new bio-based constituents and waste materials are proposed for NFC [4].

As previously mentioned, another significant benefit of NFC is their lightweight nature. Natural fibers have a lower density than synthetic

* Corresponding author.
E-mail addresses: giulia.delbianco@unicam.it (G. Del Bianco), valentina.giammaria@unicam.it (V. Giammaria), monica.capretti@unicam.it (M. Capretti), simonetta.boria@unicam.it (S. Boria), s.lenci@univpm.it (S. Lenci), raffaele.ciardiello@polito.it (R. Ciardiello), v.castorani@hpcomposites.it (V. Castorani).

https://doi.org/10.1016/j.compstruct.2024.118318
Received 28 March 2024; Received in revised form 17 May 2024; Accepted 23 June 2024
Available online 29 June 2024

fibers, resulting in a lighter composite material. This feature makes NFC particularly suitable for those applications where weight reduction is fundamental, such as in the automotive and aerospace industries. In order to meet the requirements of the European legislation – i.e., the sustainable development goals of the Agenda 2030 and 2050, including the targets for the environment, energy and climate – the lightweight contributes to fuel efficiency and lower emissions while leading to a more sustainable component. As technology advances and researchers explore new ways to optimize these materials, NFC will play a pivotal role in building a more sustainable and resilient future while respecting the environment.

In the automotive industry, the companies are increasingly incorporating these materials into the manufacturing of interior components — such as door panels, seat backs, and dashboards [5]. The eco-friendly nature of natural fibers makes them particularly appealing also in the building industry [6,7], where the environmental benefit and sustainability are increasingly becoming fundamental requirements. In particular, these composites are adopted as insulation materials [8,9] and panels for several construction applications [10]. Moreover, the end-of-life of biomass-based insulation materials in buildings is also investigated, by suggesting waste-to-energy technologies [11].

Despite the numerous advantages, NFC present several challenges and some limitations [12] — such as moisture absorption [13], aging degradation, poor interfacial adhesion between matrix and fibers, and a wide variability in the mechanical properties of the fiber [14,15], due to the different growth conditions and harvesting methods. This variability strongly affects the mechanical properties of the NFC, making it difficult to ensure consistent performance. However, ongoing research focuses on addressing these challenges through innovations in processing techniques, surface treatments [16], and the development of hybrid composites [17]. These efforts aim to enhance the mechanical performance of NFC, and extend their application fields. In particular, hybrid solutions offer a good compromise in such sense, since synthetic and natural fibers are both present as reinforcement in the polymer matrix [18,19]. In literature, several works have investigated NFC, both experimentally and numerically, also highlighting their limits [20–24]. Hence, as a first approach, these results suggest the introduction of synthetic fibers into NFC, leading to hybrid composites, to enhance their properties due to the synergic effect of the coexistence of different reinforcements. Moreover, the potential of hybridization techniques relies in the tailoring of the composites performances to satisfy specific requirements [25]. The material properties variability have also been analyzed in hybrid configurations which undergo fatigue cycles [26]. In this context, the present work aims to analyze the potential of hybrid composites in impact events, and their relative modeling, offering a complete comparison between different materials and orientations. The wide displacements that NFC offer in LVI tests is an interesting property in view of future requirements in automotive applications, although the withstood load is not comparable to carbon fiber laminates. Moreover, optimization processes are also adopted to find out the experimental unknown parameters of the material card: in particular, flax laminates subjected to LVI are already examined using this approach [27]. For this reason, a wide comparison between natural and synthetic fibers reinforced polymers is strongly required to better understand their behavior and, consequently, to identify the area where they can be applied.

Besides the type of fiber used as reinforcement, researches are also focusing on study bio-based resin system alternative to synthesized ones [28]. On the same level, they can be enriched by fillers or hardeners. Some examples are given by the polylactide acid [29], which is biodegradable and derived from corn.

On this work, the focus is on thermosetting composites, disregarding the thermoplastic ones. After an initial mechanical characterization of laminates made of carbon and flax [30] fiber fabrics, the paper aims to explore the experimental and numerical impact behavior [31,32] of these composites. In addition to the above mentioned reinforced polymers, the framework of the comparison is completed by hybrid solutions [33] impacted at the same energy levels. Moreover, for each type of material, the analyses take into account also the stacking sequence of the layers: composites with plies oriented at 0° and in a quasi-isotropic orientation are compared. A more detailed description of the materials is provided in Section 2. The tensile, compressive, and LVI tests are presented in Section 3, and then numerically solved using FE models; the description is provided in Section 4. Finally, experimental trends and numerical results are compared in Section 5.

By subjecting a material to impact under controlled conditions, its ability to absorb and dissipate energy can be evaluated, as well as its overall toughness and durability. The knowledge of this behavior enables to select the right material in the design phase depending on the application in which it will be used, based on its ability to withstand impact forces. For example, in the automotive industry, LVI tests are used to evaluate the crashworthiness of vehicles and their components. By simulating impacts at low velocities, the structural integrity can be verified, ensuring that they meet safety requirements. Moreover, failure modes can determine and influence energy absorption capabilities; in particular, natural fibers strongly differ from synthetic ones, showing fibrils and nonlinear behavior [34]. In order to compare the energy absorption capability of the materials taken into account in the present work, the SEA is investigated in Section 3.2.

2. Materials

Four different types of reinforced polymers are experimentally investigated, and then numerically modeled, starting from carbon (C) and flax (F) fibers. In addition to single material configurations, two hybrid solutions are proposed as case study for the LVI tests: carbon-flax-carbon (CFC), and flax-carbon-flax (FCF). Both the fibers are woven in a balanced twill 2 × 2 architecture, and they are embedded in the same toughened epoxy resin, resulting in a PrePreg roll. The laminates characteristics – namely, fabric grammage, resin content (RC), and fiber volume fraction (FVF) – are the following: Carbon: 380 g/m^2, RC = 38%, FVF = 58%, Flax: 350 g/m^2, RC = 52%, FVF = 41%.

All the samples were manufactured by HP Composites SpA, by stacking 8 layers of these PrePregs with the same orientation. As regards both hybrid composites, the central core is composed of four layers, while the two outer layers on the same side are of different reinforcement material; thus, CFC stands for $C_2F_4C_2$, and FCF refers to $F_2C_4F_2$. In particular, the tensile and compressive tests are based on single material specimens oriented at 0° and 90°– $[0]_8$ and $[90]_8$, respectively – to obtain their respective mechanical properties; the 45° orientation $[45]_8$ has been taken into account for the shear properties in tensile tests, too. Instead, two different stacking sequences are investigated for the LVI tests: the first refers to the plies placed at 0° orientation, and the other consists of a quasi-isotropic orientation — i.e., $[0]_8$ and $[0_3/+45/–45/90/0_2]$, respectively. The laminates curing process takes places in autoclave at 135 °C and 6 bar for 90 min, under a vacuum bag of −1 bar, with an initial heating ramp (rate of 3 °C/min) and a final cooling ramp (rate of 4 °C/min) to ensure uniform temperature distribution and avoid sample deformation.

The overall average thickness of the composites are listed below: 3.36 mm for carbon, 4.96 mm for flax, and 4.00 mm for hybrid. In particular, since the fabrics crimping of the overlapping layers is different, it is important to remark that the values differ between 0° and ISO orientations, leading to a greater thickness in this last case due the layers oriented at 45°. From these, the resulting average thickness of each ply is equal to 0.42 mm and 0.62 mm, for carbon and flax respectively. In particular, these are the values adopted for the materials numerical modeling in Section 4.

Table 1
Experimental tensile properties of carbon and flax specimens. E_t: Young modulus; $\sigma_{u,t}$: tensile strength; G: shear modulus; τ_u: shear strength; $\epsilon_{u,t}$: ultimate strain; $\epsilon_{u,s}$: ultimate shear strain.

	E_t [GPa]	$\sigma_{u,t}$ [MPa]	G [GPa]	τ_u [MPa]	$\epsilon_{u,t}$	$\epsilon_{u,s}$
Carbon	59.4 ± 2.9	993 ± 9	3.3 ± 0.1	58 ± 0	0.016	0.050
Flax	9.9 ± 0.6	138 ± 14	1.7 ± 0.1	40 ± 1	0.018	0.085

Table 2
Experimental compressive properties of carbon and flax specimens. E_c: Young modulus; $\sigma_{u,c}$: compressive strength; $\epsilon_{u,c}$: ultimate strain.

	E_c [GPa]	$\sigma_{u,c}$ [MPa]	$\epsilon_{u,c}$
Carbon	57.4 ± 2.5	468 ± 15	0.009
Flax	9.0 ± 0.2	99 ± 8	0.077

Table 3
Mode I (G_{IC}) and Mode II (G_{IIC}) interlaminar fracture toughness.

	G_{IC} [J/m^2]	G_{IIC} [J/m^2]
Carbon	2108.6	1810.7
Flax	2000.8	1974.0

3. Experimental tests

3.1. Tensile and compressive tests

Firstly, the mechanical characterization of carbon and flax laminates is carried out through tensile and compressive tests.

According to the ASTM D3039 standard, the tensile tests are performed on 250 mm × 25 mm rectangular specimens with a test speed of 2 mm/min. For both material configurations, the grips length is 60 mm on each side; the unconstrained portion of the samples is therefore equal to 130 mm.

Compressive tests are conducted in accordance with the following standards, depending on the reinforcement material and its failure mode: ASTM D6641 for carbon laminates on 140 mm × 25 mm rectangular specimens with a test speed of 1 mm/min, and ASTM D695 for flax laminates on 80 mm × 13 mm rectangular specimens with a test speed of 1.3 mm/min. The tests have involved a free portion of length 13 mm for carbon, and 20 mm for flax. Buckling phenomena are observed in both materials, especially in flax laminates, which undergo a major plastic deformation before failure.

The tensile and compressive properties are summarized in Tables 1 and 2, respectively. The experimental load–displacement curves of both tests are instead shown in Section 5, coupled with the corresponding numerical results. For each specific configuration, 5 carbon samples and 4 flax samples have been tested for tensile tests; 3 carbon samples and 2 flax samples have been tested for compressive tests, instead.

The tests described above mechanically characterize the fibers of the laminates. In addition to these, Double Cantilever Beam (DCB) and 4-point End Notched Flexure (4ENF) tests have also been conducted to study the matrix properties – i.e., the energy release rate of the epoxy resin – according to the ASTM D5528 and ASTM D7905 standards, respectively. The resulting Mode I and Mode II interlaminar fracture toughness are therefore reported in Table 3.

3.2. Low-Velocity Impact (LVI) tests

Laminate test plates of dimension 100 mm × 100 mm are impacted at five different energy levels, depending on the materials. As mentioned in Section 2, two different stacking sequences of the laminates are taken into account for each material to have a complete comparison. Carbon samples along with both CFC and FCF hybrid laminates are tested at 20 J, 30 J, 40 J, 50 J, and 55 J, corresponding to a dart impact velocity of 1.59 m/s, 1.97 m/s, 2.28 m/s, 2.54 m/s, and 2.67 m/s, respectively. Since flax laminates hold a lower impact resistance, the samples reinforced in fully flax are subjected to lower impact energy levels: 10 J, 15 J, 20 J, 30 J, and 40 J, corresponding to a dart impact velocity of 1.13 m/s, 1.38 m/s, 1.59 m/s, 1.97 m/s, and 2.28 m/s, respectively. The drop tower machine (Instron/CEAST Fractovis Plus) is equipped with a hemispherical impactor tip of 20 mm diameter and a total mass of 15.89 kg, which is left constant for all the tests. By varying the impactor height, the impact energies are reproduced. Finally, two steel plates with a circular opening of 76 mm diameter are the boundary conditions of the test machine, through which the samples are clamped in an interlocking constraint.

Table 4
Absorbed energies by samples during LVI tests.

	Carbon		Flax		CFC		FCF	
	0°	ISO	0°	ISO	0°	ISO	0°	ISO
10 J	–	–	5.8	5.7	–	–	–	–
15 J	–	–	10.0	10.3	–	–	–	–
20 J	13.2	13.8	14.5	13.8	17.6	17.0	11.6	15.3
30 J	22.3	25.6	26.6	22.8	28.1	27.5	23.8	26.7
40 J	35.2	36.5	35.3	30.9	39.5	38.9	36.9	38.4
50 J	46.1	47.6	–	–	49.3	49.6	48.8	49.1
55 J	51.7	53.5	–	–	–	54.6	54.3	53.8

The resulting load–displacement curves of both orientations are shown in Figs. 1 for carbon, in Figs. 2 for flax, in Figs. 3 for CFC, and in Figs. 4 for FCF, respectively. In LVI tests, the displacements vectors – i.e., those reported in the graphs, for each material configurations and orientations – are obtained through a double integration of the equilibrium equation, starting from the initial velocity of the dart [35].

The energies absorbed by the test pieces are reported in Table 4. By associating these values with the respective experimental trends, it is possible to highlight the following evidence: energies are the same between the 0° and ISO orientations, although the hysteresis curves are distributed differently, and this is true for each material configuration. In particular, the 0° orientations offer higher peak force with a minor displacement, while ISO orientations reduce the load to promote a greater elongation. In relation to Table 4, the only significantly difference in values can be found in flax laminates impacted at 20 J. Similar conclusions are also drawn from the comparison between CFC and FCF hybrid laminates oriented at 0°, although their elongations are comparable. More in detail, CFC samples can withstand a lower force while ensuring a global plateau trend; instead, FCF shows an initial load peak and, therefore, a variation in the bearing capability. In order to design an energy absorber component, these considerations suggest that the first condition is preferable, since it ensures a better stability during the impact phase due to the constant level of force to which the specimens are attested. In particular, for this reason, all the ISO orientations deserve a further investigation in such sense. For example, it can be seen how the ISO curves greatly differ from those at 0° especially in Figs. 1 and Figs. 4, for carbon and FCF configurations respectively, where a greater displacement is reached.

In order to compare the energy absorption capability of the materials, the SEA evaluation is carried out. The values are obtained as the ratio between the average absorbed energy (please, see Table 4) and the destroyed mass. This latter, in particular, refers to the mass of the central cylinder, associated to the unconstrained impact area of 76 mm diameter – i.e., the one interested in absorbing energy – and it is calculated as the density of the material multiplied by the volume of this cylinder. Figs. 5 and 6 provide a comparison of the performance for all the tested materials.

Figs. 7 and 8 report the damage propagation on specimens' surfaces oriented at 0°, highlighting the same failure mechanisms in the different materials: i.e., as the impact energy increases, the rear of samples exhibit a growing cross-shaped damage, and the front faces show the increasingly visible imprint given by the dart fall. In particular, the visual inspection focuses on 3 energy levels, depending on

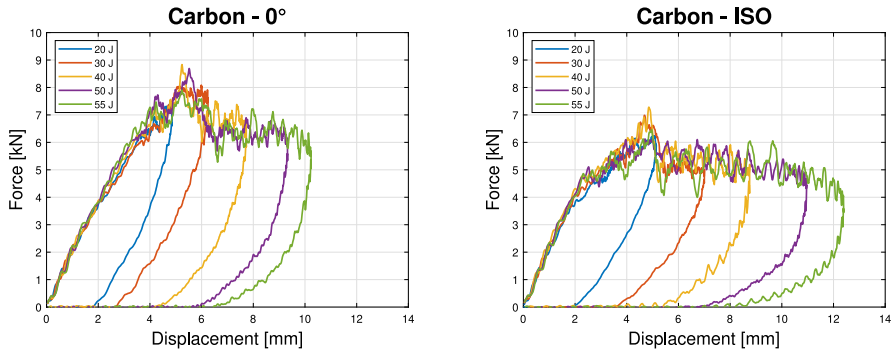

Fig. 1. Experimental load–displacement curves of LVI tests: carbon samples with (a) 0°, and (b) quasi-isotropic orientation.

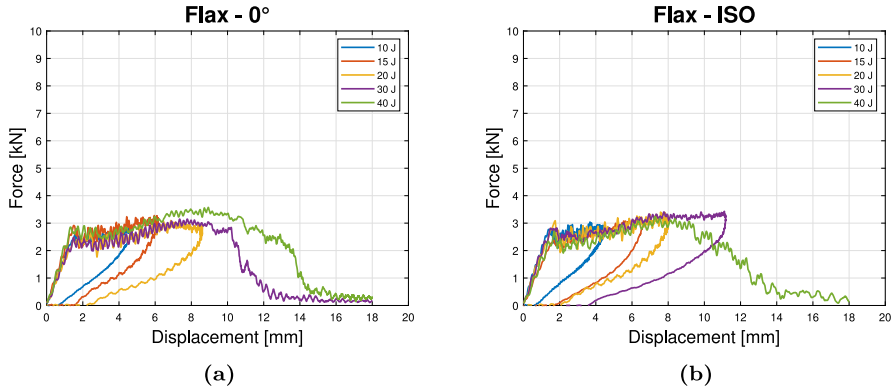

Fig. 2. Experimental load–displacement curves of LVI tests: flax samples with (a) 0°, and (b) quasi-isotropic orientation.

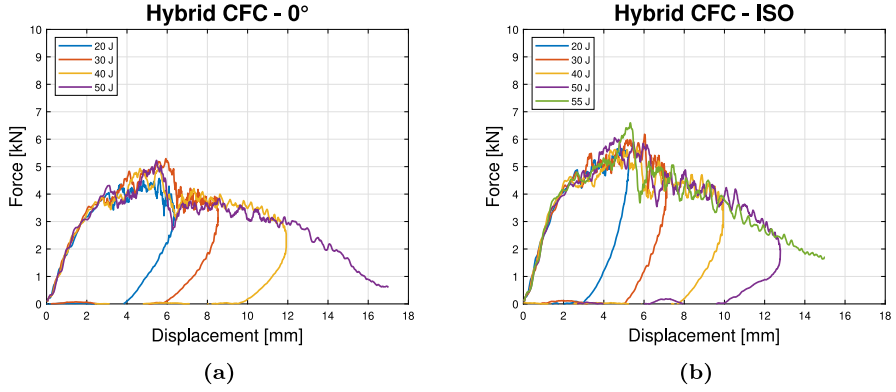

Fig. 3. Experimental load–displacement curves of LVI tests: hybrid CFC samples with (a) 0°, and (b) quasi-isotropic orientation.

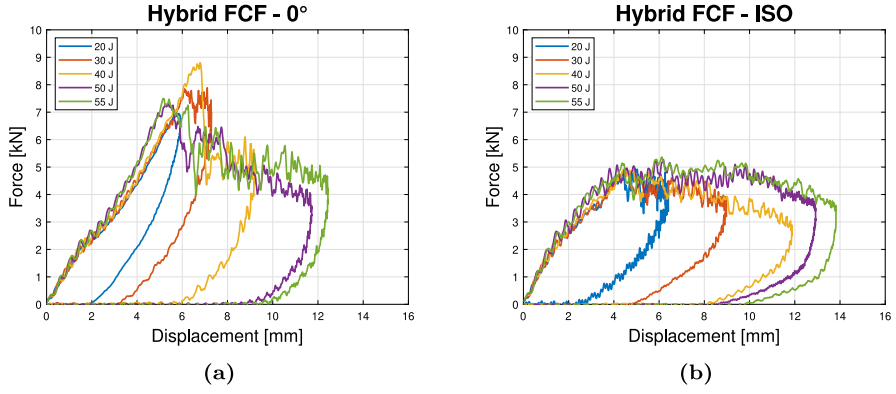

Fig. 4. Experimental load–displacement curves of LVI tests: hybrid FCF samples with (a) 0°, and (b) quasi-isotropic orientation.

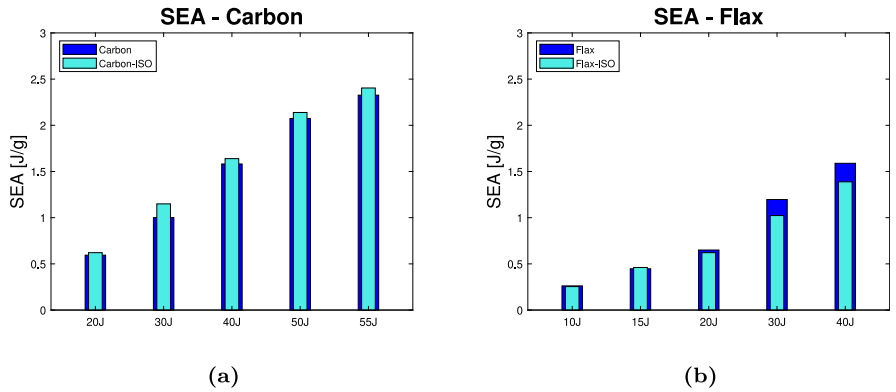

Fig. 5. SEA evaluation: (a) Carbon, and (b) Flax.

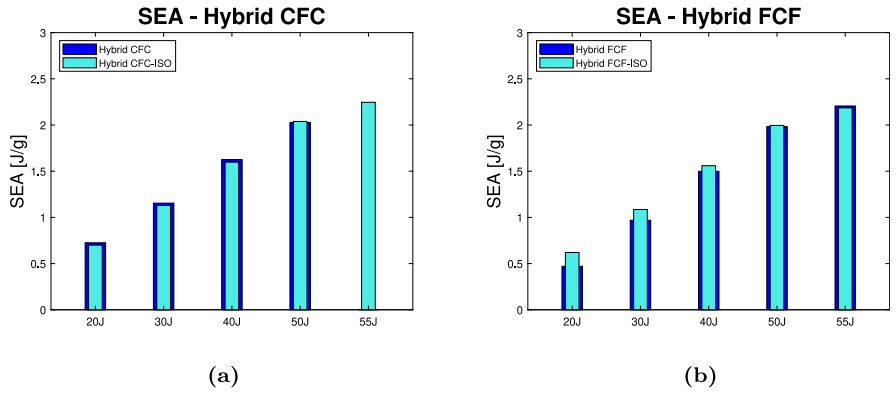

Fig. 6. SEA evaluation: hybrid (a) CFC, and (b) FCF.

the material: the minimum, the average, and the maximum common ones. The same energy levels are then numerically investigated and reported in Section 5, along with the damage comparison. As expected, when comparing both hybrid composites to pure material laminates, the extent of the damage is larger than that of carbon ones, and, on the other hand, much smaller than that of flax ones. More in detail, when comparing the two different hybrid configurations each other, it can be noted how the CFC samples ensures a slightly less damaged and compacted area with respect to the FCF ones, especially in the back surfaces. This phenomenon can be explained by the carbon fiber reinforcement in the outer layers, which allows for a more brittle failure. Similarly, the outer layers of flax in the FCF configuration shows a more visible and extensive damage, since the fiber is natural, and so more weak; in particular, this aspect can be attributable to the peak loads observed in the experimental hysteresis curves.

4. Numerical modeling

The FE models of the experimental tests presented in Section 3 are initially created using Altair HyperMesh software. FE analyses are then performed through the LS-DYNA solver [36].

As previously mentioned in Section 2, the thickness of each modeled ply is equal to 0.42 mm for carbon, and 0.62 mm for flax.

The most commonly used material card for modeling reinforced composites on LS-DYNA is MAT54/55 (MAT_ENHANCED_COMPOSITE_DAMAGE), which is designed to reproduce the brittle behavior of a unidirectional material, linear up to failure. Another interesting material model is MAT58 (MAT_LAMINATED_COMPOSITE_FABRIC), since it is developed to model composite materials with woven fabrics. The failure criterion is Chang–Chang for MAT54/55, while MAT58 handle the failure surface type (FS) through a variable in the material card. In this study, FS parameter is assumed to be 1, and so it means that a smooth failure surface with a quadratic criterion for both the longitudinal and transverse directions is applied. Moreover, an interaction between normal and shear stresses is assumed for the evolution of damage in both these directions. For a detailed description and comparison of the material models available in LS-DYNA to describe the behavior of composite materials, as well as the failure criteria and required parameters, please see the manual [36] and the article by Rabiee [37]. In this paper, the behavior of the composites is described using the MAT54/55 material model for carbon plies, and the MAT58 for flax plies, according to the experimental values presented in Section 3. This MAT58 material card is adopted to model woven natural fibers composites, since it is better able to reproduce the elasto-plastic trend of natural fibers in the load–displacement plots, and therefore preferable to MAT54/55. In particular, a detailed analyses of the failure mechanism of flax fiber is provided by Ahmed [34]: the initial nonlinear behavior, typical of natural fibers, is related to their viscoelastic nature and to the rearrangement of fibrils.

The numerical models of the tensile and compressive tests are created using shell elements under the same quasi-static conditions, starting from the real specimen dimensions. For both tests, they consist of 1 composite layer, to which the stacking sequence is assigned in PART_COMPOSITE. The mesh size is 1 mm for tensile model; for compression, instead, the elements are of 1 mm for carbon and 0.5 mm for flax, due to the smaller dimension of the physical samples. Once the sample is modeled, the boundary condition of prescribed motion is imposed to one edge – i.e., to the set of nodes tab corresponding to the varying grip length depending on the test – while a set of nodes of the same size is constrained for translations and rotations on the opposite site. Moreover, the set of the moving nodes is also constrained for translations and rotations, with the only degree of freedom in the movement direction.

The numerical model for the LVI tests, shown in Fig. 9, consists of 4 composite shell layers, each of which with two integration points

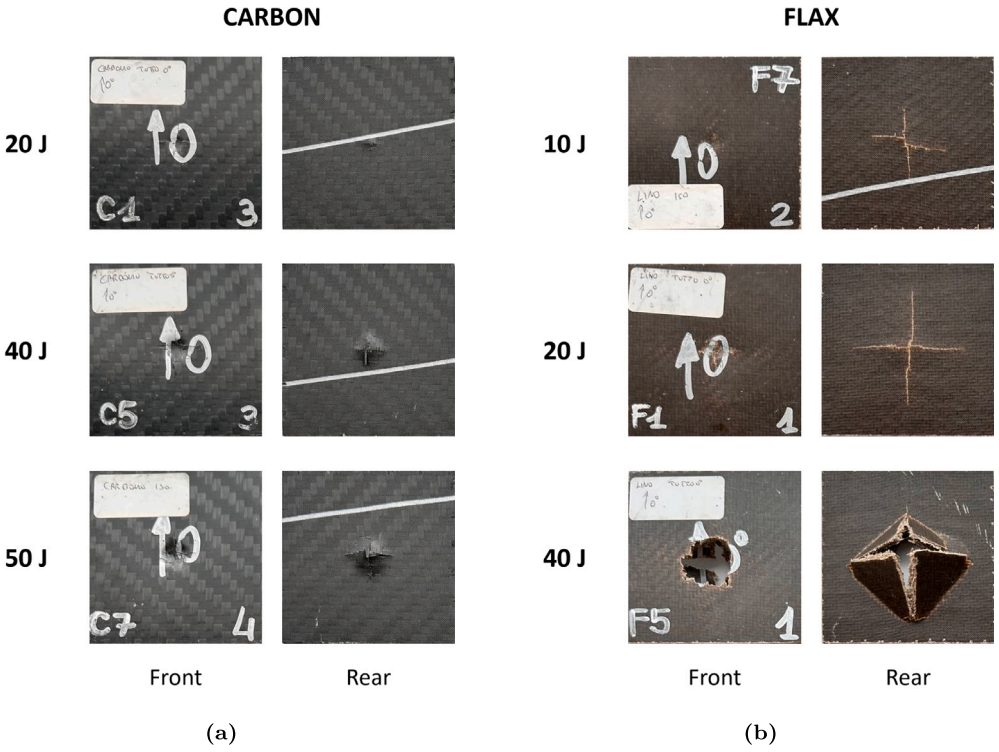

Fig. 7. Experimental damage progression on laminates surfaces impacted at different energy levels: (a) Carbon, and (b) Flax samples oriented at 0°.

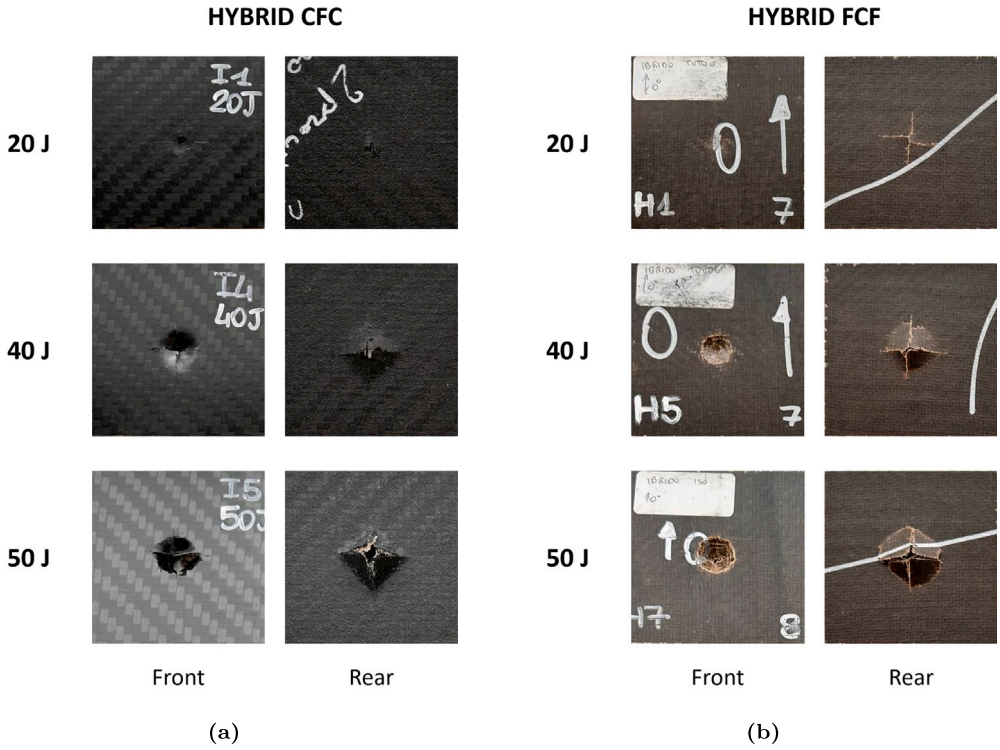

Fig. 8. Experimental damage progression on hybrid laminates surfaces impacted at different energy levels: (a) CFC, and (b) FCF samples oriented at 0°.

through the thickness to reproduce the 8 layers of the real specimens. The interlocking boundary conditions are prescribed to the nodes outside the impact zone of 76 mm: all the degrees of freedom are constrained, by blocking translations and rotations. The spherical impactor of 20 mm diameter is modeled as a rigid body with solid elements using the MAT20 (MAT_RIGID) material card. The total mass assigned to the sphere is 15.89 kg, equal to that of the experimental tests. Finally, the respective initial dart velocities – which correspond to the tested energy levels – are imposed as initial conditions of the sphere.

A proper contact modeling needs to be defined to best reproduce the impact phenomenon and the delamination of the sample

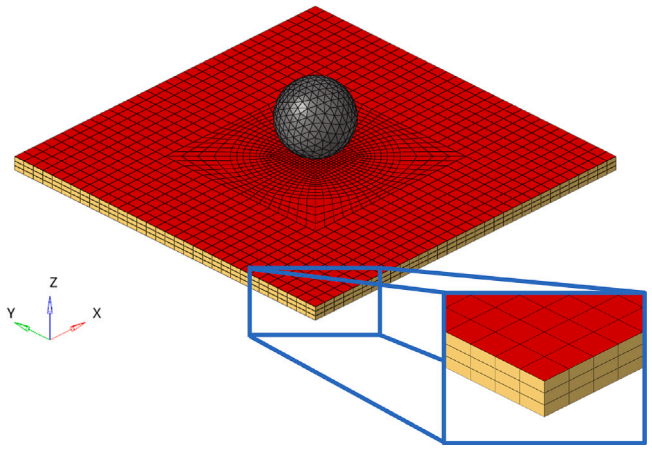

Fig. 9. Numerical impact model, with a close-up of the 4 shell layers connected by the 3 solid cohesive layers.

Table 5
MAT54/55 Material card for carbon plies. Moduli and strengths are expressed in GPa, density in kg/mm^3.

MAT_ENHANCED_COMPOSITE_DAMAGE (MAT54/55)				
RO	**EA**	**EB**	**PRBA**	
1.44 E-6	60	60	0.03	
GAB	**GBC**	**GCA**	**2WAY**	
3.3	3.3	3.3	1	
DFAILM	**DFAILS**	**DFAILT**	**DFAILC**	
0	0.104	0.083	−0.074	
XC	**XT**	**YC**	**YT**	**SC**
0.47	0.99	0.47	0.99	0.06

plies: firstly, one contact (CONTACT_SURFACE_TO_SURFACE) is imposed between the sphere and the laminate to analyze the interaction between the master and slave surfaces during the impact. Then, the single surface contact (CONTACT_AUTOMATIC_SINGLE_SURFACE) helps to avoid the interpenetration of the elements, involving the whole slave part. Then, the four plies of the composite are each other connected by three layers of cohesive solid elements, to which the MAT138 (MAT_COHESIVE_MIXED_MODE) material card is associated. Compared to the widely used tiebreak contacts, the cohesive modeling allows to better describe the interlaminar interactions; in particular, the fracture toughness values of G_{IC} and G_{IIC}, reported in Table 3, are inserted inside the card. Unlike the parameters that handle the tiebreak card, since experimental values can be directly used in the cohesive card – without adversely affecting the computational costs related to a thin solid mesh of the elements –, the choice to adopt a cohesive modeling results preferable to the tiebreak contacts between the laminate plies. For clarity, in Fig. 9, these solid elements hide the material shell layers from the view.

The same model is adopted for all material configuration and for all impact energy cases, by changing the initial velocity of the sphere, the thickness and the orientation of the layers, along with the properties of the MAT54/55 and MAT58 material cards.

5. Results and discussion

In the same order as they are presented in Section 3, the experimental results are here compared with the numerical ones.

Tables 5 and 6 summarize the parameters of the two material cards: as described in Section 4, they are MAT54/55 for carbon, and MAT58 for flax, respectively. In particular, the 2WAY parameter in MAT54/55 enables to consider fiber behavior in both longitudinal and transverse directions, as a woven fabric.

Table 6
MAT58 Material card for flax plies. Moduli and strengths are expressed in GPa, density in kg/mm^3.

MAT_LAMINATED_COMPOSITE_FABRIC (MAT58)				
RO	**EA**	**EB**	**PRBA**	
1.27 E-6	10	10	0.12	
GAB	**GBC**	**GCA**	**ERODS**	**FS**
1.7	1.7	1.7	0.25	1
E11C	**E11T**	**E22C**	**E22T**	**GMS**
0.08	0.02	0.08	0.02	0.08
XC	**XT**	**YC**	**YT**	**SC**
0.1	0.13	0.12	0.15	0.04

As regards mechanical characterization on carbon and flax laminates, the computation of tensile and compressive models allows to calibrate the material card parameters correctly, depending on the experimental properties. The load–displacement curves comparisons between experimental tests and numerical models are presented below. In particular, Figs. 10 and 11 illustrate the tensile results of carbon and flax, respectively; similarly, Figs. 12 and 13 refers to the compressive tests. Since both fabrics are balanced, the same results are numerically obtained for 0° and 90° orientations.

From the experimental point of view, instead, the compression of flax deserves a remark: a slight difference can be observed between the curves in 90° orientation, hence no correct reproducibility is reached. Relying on the above mentioned bucking phenomenon (please, see Section 3), along with the number of tested specimens, the problem can be attributed to the testing phase or in production technique, and, therefore, new further analyses need to be done in the future. Moreover, the presence of fibrils, typical of natural fibers, generates a macroscopic variable failure modes from case to case in the samples, depending on the microscopic single fiber fraying mode in the yarn of the fabric.

With respect to LVI tests, the numerical investigation has involved part of the material configurations — i.e., carbon, flax, and hybrid CFC. To summarize the behaviors of each of these, the criterion was to choose 3 energy levels, as previously mentioned in Section 3.2: the minimum, the average, and the maximum common ones. Figs. 14 and 15 show the load–displacement curves comparison for carbon plates in both 0° and ISO configurations, respectively. In the same way, Figs. 16 and 17 provide the experimental and numerical LVI curves for flax laminates, and, finally, Figs. 18 and 19 refer to the results of hybrid CFC, in both 0° and ISO configurations, respectively.

The numerical hysteresis curves are similar to the experimental ones, although the presence of some load peaks, common to all the results. In particular, the following evidence can be highlighted in both 0° and ISO materials orientations: on the one hand, carbon models exhibit a numerical greater load in the final part of the linear phase with respect to the experimental curves; on the other, the same trend to overestimate the load is also found in flax models, but in the subsequent plastic phase, with oscillations due to a noisy load. As regards the terminal part of the curves, in those cases where no perforation of the test pieces has occurred, the spring back phase is numerically well reproduced.

Alongside to these results, a damage analysis has also been conducted to validate the model ability to reproduce the experimental failure mode of the samples. Figs. 20 show the comparison between experimental and numerical cross-shaped damages on carbon laminates impacted at 50 J, from which the stress distribution in the two directions is clearly visible in both front and rear surface.

6. Conclusions

The present paper provides a comprehensive experimental and numerical investigation of composites subjected to LVI tests. The analyses are conducted on different types of reinforcement — namely, flax, carbon, and hybrid flax-carbon (CFC and FCF) laminates. The impact

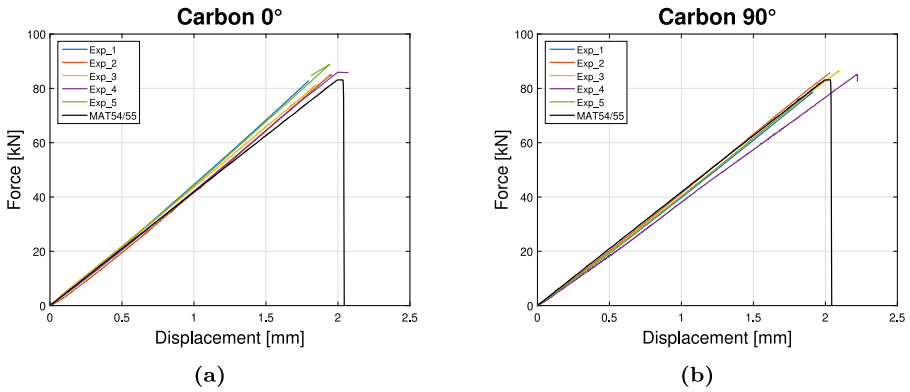

Fig. 10. Experimental and numerical load–displacement curves of tensile tests: carbon samples oriented at (a) 0°, and (b) 90°.

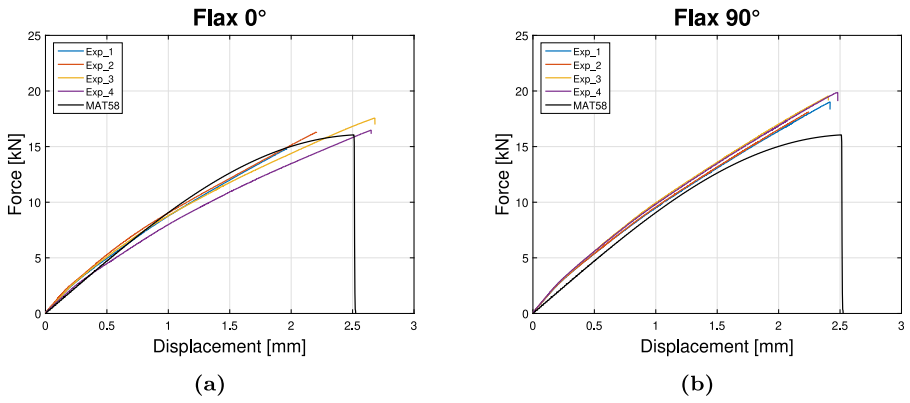

Fig. 11. Experimental and numerical load–displacement curves of tensile tests: flax samples oriented at (a) 0°, and (b) 90°.

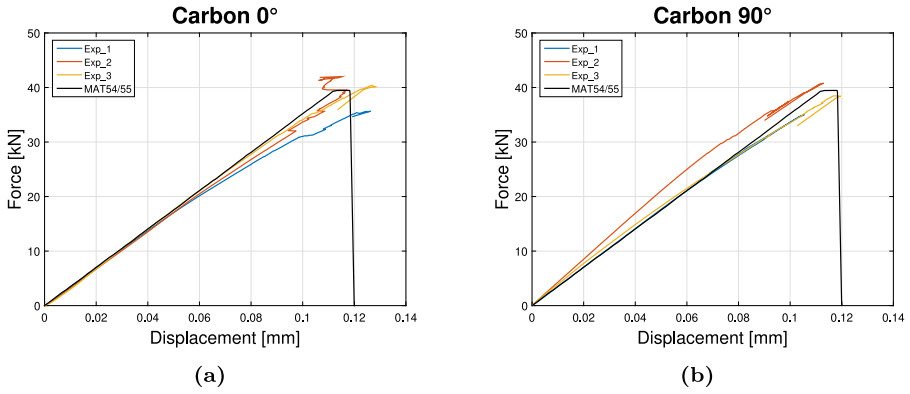

Fig. 12. Experimental and numerical load–displacement curves of compressive tests: carbon samples oriented at (a) 0°, and (b) 90°.

energy levels to which the specimens are subjected to are chosen according to the material strength, and overall are the following: 10 J, 15 J, 20 J, 30 J, 40 J, 50 J, and 55 J. In particular, only the samples reinforced in fully flax are subjected to lower impact energy levels. To properly model the different nature of these reinforcement fibers, two different LS-DYNA material cards are adopted — i.e., MAT54/55 for carbon plies, and MAT58 for flax plies, respectively. More specifically, the MAT54/55 is designed to reproduce the linear behavior until failure, typical of brittle materials, and the MAT58 better describes the nonlinear counterpart of natural fibers. A first mechanical characterization has involved tensile and compressive tests on carbon and flax fiber composites, from which the material model parameters are properly calibrated, according to both experimental computed properties and observed behaviors. Subsequently, the material cards thus obtained are successfully employed in the LVI numerical models, to predict the composite laminates responses at different energy levels, allowing for a good reproduction of the experimental load–displacement curves.

By associating the energies absorbed by the specimens during LVI with the respective experimental trends, the following evidence has been found for each material configuration. No significant differences are detected when changing the fiber orientation – i.e., from 0° to the ISO configuration –, although the hysteresis curves are differently distributed in the load–displacement graphic, and hence their shapes do not overlap. More in detail, the 0° orientations offer higher load peaks coupled with a minor maximum displacements, while the ISO orientations reduce the load to promote instead a greater elongation. Similar conclusions are also drawn from the comparison between hybrid laminates (CFC and FCF) oriented at 0°, although their elongations are comparable. In particular, CFC samples can withstand a lower force while ensuring a global plateau trend; instead, FCF shows an initial load

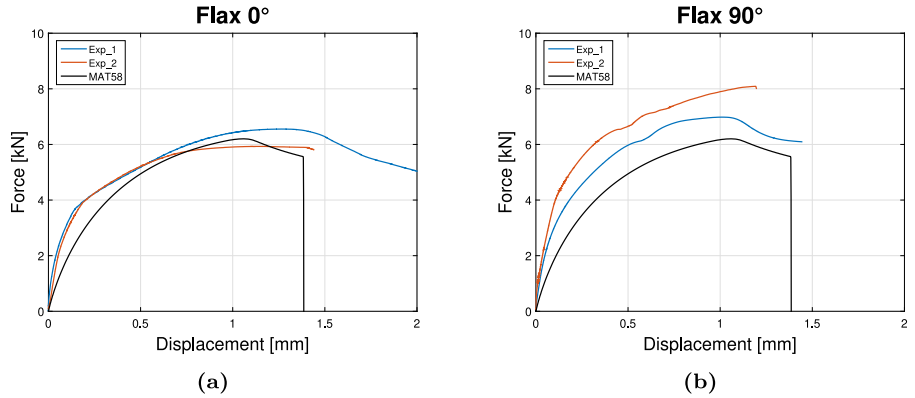

Fig. 13. Experimental and numerical load–displacement curves of compressive tests: flax samples oriented at (a) 0°, and (b) 90°.

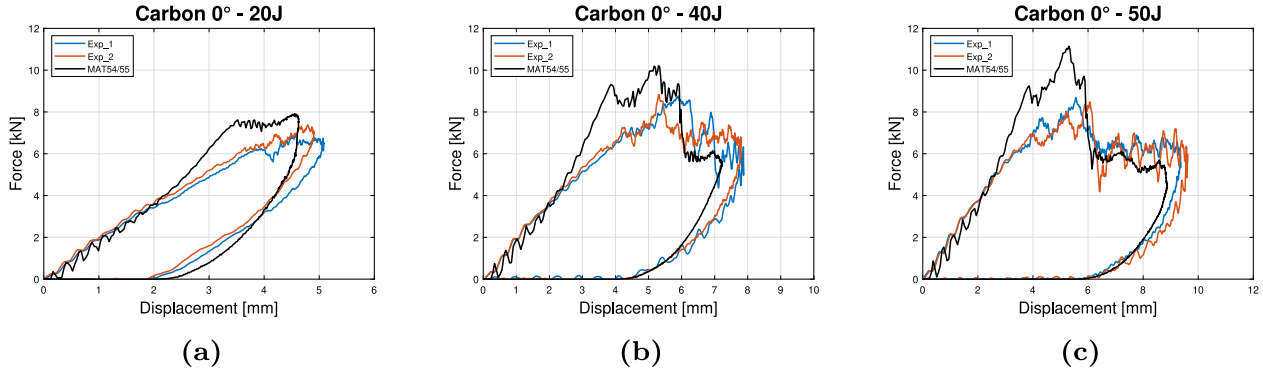

Fig. 14. Experimental and numerical load–displacement curves of LVI tests: carbon samples oriented at 0° impacted at (a) 20 J, (b) 40 J, and (c) 50 J.

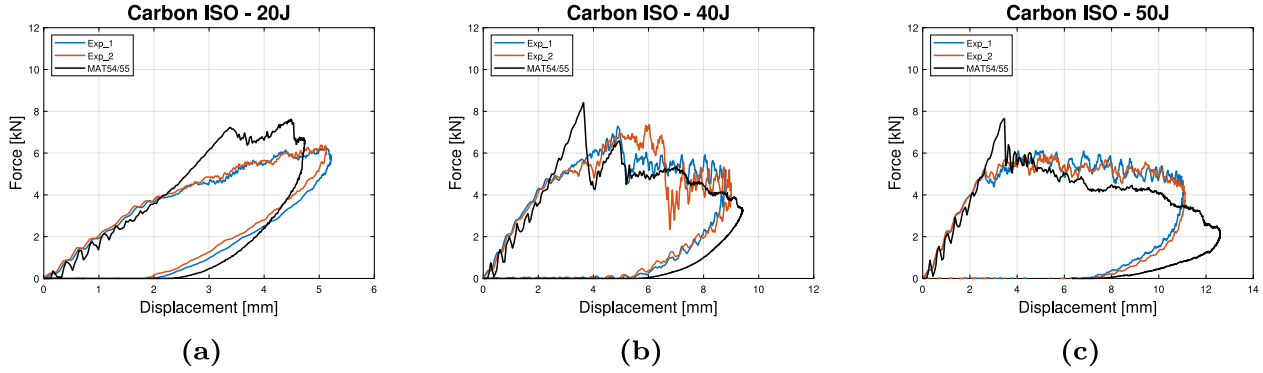

Fig. 15. Experimental and numerical load–displacement curves of LVI tests: carbon samples with quasi-isotropic orientation impacted at (a) 20 J, (b) 40 J, and (c) 50 J.

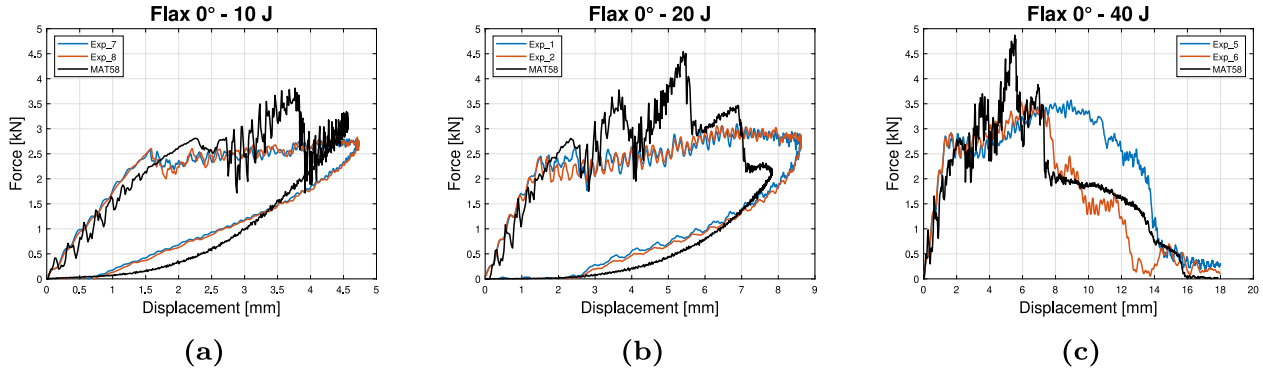

Fig. 16. Experimental and numerical load–displacement curves of LVI tests: flax samples oriented at 0° impacted at (a) 10 J, (b) 20 J, and (c) 40 J.

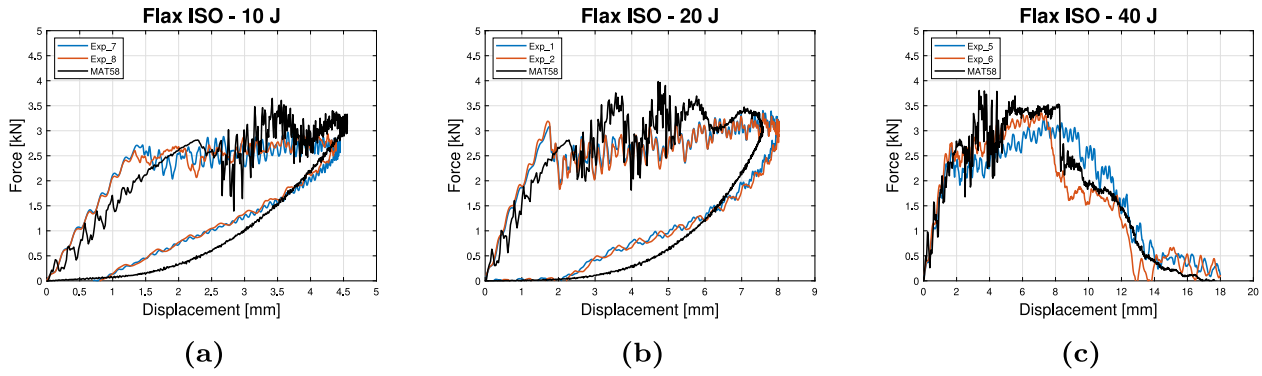

Fig. 17. Experimental and numerical load–displacement curves of LVI tests: flax samples with quasi-isotropic orientation impacted at (a) 10 J, (b) 20 J, and (c) 40 J.

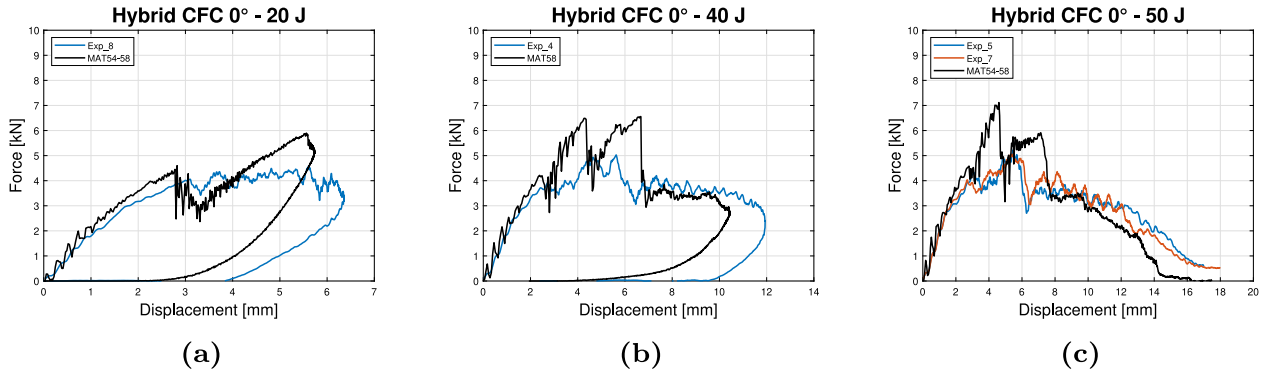

Fig. 18. Experimental and numerical load–displacement curves of LVI tests: hybrid CFC samples oriented at 0° impacted at (a) 20 J, (b) 40 J, and (c) 50 J.

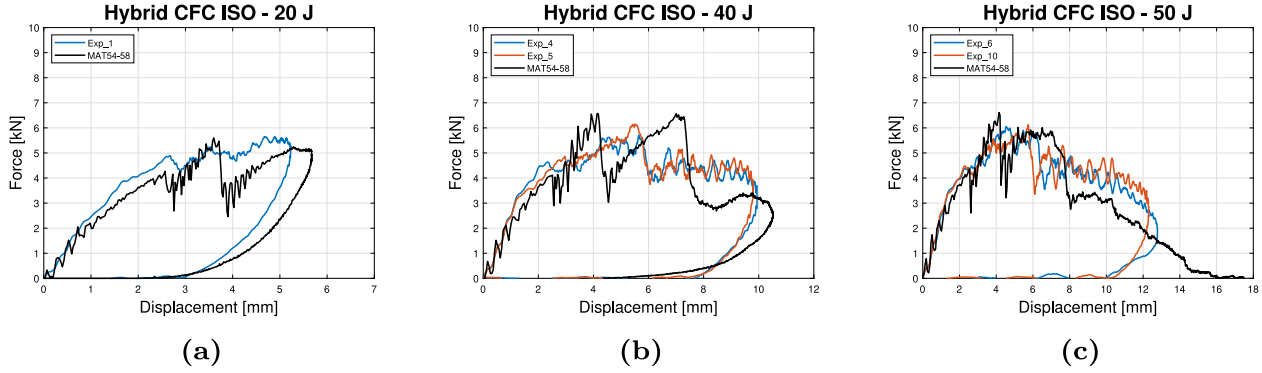

Fig. 19. Experimental and numerical load–displacement curves of LVI tests: hybrid CFC samples with quasi-isotropic orientation impacted at (a) 20 J, (b) 40 J, and (c) 50 J.

peak and, therefore, a variation in the bearing capability. In conclusion, the overall energy performances are resulted comparable. Anyway, in order to design an energy absorber component, the obtained results indicates the first condition as preferable, since it ensures a better stability during the impact phase, due to the constant level of force to which the specimens are attested.

When comparing the energy absorption capability, neither flax nor hybrids reinforcements achieve comparable values to carbon ones, which clearly exhibit the highest SEA values in each impact energy level. However, both hybrid configurations (CFC and FCF) are showed promising and satisfactory results for the above-mentioned reasons. From a crashworthiness perspective, in the design process of a component, the key aspects to be taken into account concern the energy absorption capability and the distribution of the hysteresis curve in terms of load and displacement, with a special focus to maintaining a maximum load plateau during impact events as constant as possible. In this regard, ISO orientations ensure a greater stability for each tested material, and, for this reason, they deserve a further investigation in such sense.

CRediT authorship contribution statement

Giulia Del Bianco: Writing – original draft, Writing – review & editing, Visualization, Validation, Investigation, Methodology, Formal analysis, Data curation. **Valentina Giammaria:** Writing – review & editing, Visualization, Validation, Investigation, Methodology, Formal analysis, Data curation. **Monica Capretti:** Writing – review & editing, Visualization, Validation, Investigation, Formal analysis, Data curation. **Simonetta Boria:** Writing – review & editing, Supervision, Project administration, Investigation, Conceptualization. **Stefano Lenci:** Writing – review & editing, Supervision, Conceptualization. **Raffaele Ciardiello:** Writing – review & editing, Investigation. **Vincenzo Castorani:** Writing – review & editing, Investigation, Conceptualization, Resources.

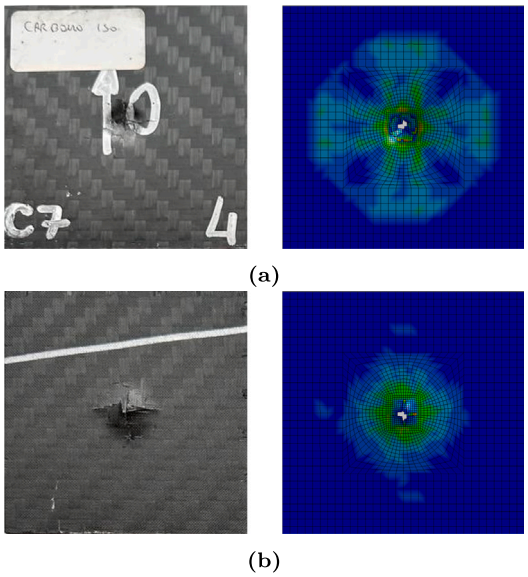

Fig. 20. Experimental and numerical damage progression on carbon laminates surfaces impacted at 50 J: (a) front, and (b) rear.

Declaration of competing interest

The authors declare the following financial interests/personal relationships which may be considered as potential competing interests: Vincenzo Castorani reports a relationship with HP Composites that includes: employment. The other authors declare that they have no known competing financial interests or personal relationships that could have appeared to infuence the work reported in this paper.

Data availability

Data will be made available on request.

References

[1] Peças P, Carvalho H, Salman H, Leite M. Natural fibre composites and their applications: A review. J Compos Sci 2018;2(4):66. http://dx.doi.org/10.3390/jcs2040066.

[2] Sarikaya E, Çallioğlu H, Demirel H. Production of epoxy composites reinforced by different natural fibers and their mechanical properties. Composites B 2019;167:461–6. http://dx.doi.org/10.1016/j.compositesb.2019.03.020.

[3] Gurunathan T, Mohanty S, Nayak SK. A review of the recent developments in biocomposites based on natural fibres and their application perspectives. Composites A 2015;77:1–25. http://dx.doi.org/10.1016/j.compositesa.2015.06.007.

[4] Väisänen T, Das O, Tomppo L. A review on new bio-based constituents for natural fiber-polymer composites. J Clean Prod 2017;149:582–96. http://dx.doi.org/10.1016/j.jclepro.2017.02.132.

[5] Park G, Park H. Structural design and test of automobile bonnet with natural flax composite through impact damage analysis. Compos Struct 2018;184:800–6. http://dx.doi.org/10.1016/j.compstruct.2017.10.068.

[6] Dahy H. Natural fibre-reinforced polymer composites (NFRP) fabricated from lignocellulosic fibresfor future sustainable architectural applications, case studies: Segmented-shell construction, acoustic panels, and furniture. Sensors 2019;19(3):738. http://dx.doi.org/10.3390/s19030738.

[7] Sassoni E, Manzi S, Motori A, Montecchi M, Canti M. Novel sustainable hemp-based composites for application in the building industry: Physical, thermal and mechanical characterization. Energy Build 2014;77:219–26. http://dx.doi.org/10.1016/j.enbuild.2014.03.033.

[8] Erkmen J, Yavuz HI, Kavci E, Sari M. A new environmentally friendly insulating material designed from natural materials. Constr Build Mater 2020;255:119357. http://dx.doi.org/10.1016/j.conbuildmat.2020.119357.

[9] Asdrubali F, D'Alessandro F, Schiavoni S. A review of unconventional sustainable building insulation materials. Sustain Mater Technol 2015;4:1–17. http://dx.doi.org/10.1016/j.susmat.2015.05.002.

[10] Sinka M, Korjakins A, Bajare D, Zimele Z, Sahmenko G. Bio-based construction panels for low carbon development. Energy Procedia 2018;147:220–6. http://dx.doi.org/10.1016/j.egypro.2018.07.063.

[11] Rabbat C, Awad S, Villot A, Rollet D, Andrès Y. Sustainability of biomass-based insulation materials in buildings: Current status in France, end-of-life projections and energy recovery potentials. Renew Sustain Energy Rev 2022;156:111962. http://dx.doi.org/10.1016/j.rser.2021.111962.

[12] Gholampour A, Ozbakkaloglu T. A review of natural fiber composites: properties, modification and processing techniques, characterization, applications. J Mater Sci 2020;55(3):829–92. http://dx.doi.org/10.1007/s10853-019-03990-y.

[13] Moudood A, Rahman A, Öchsner A, Islam M, Francucci G. Flax fiber and its composites: An overview of water and moisture absorption impact on their performance. J Reinf Plast Compos 2019;38(7):323–39. http://dx.doi.org/10.1177/0731684418818893, Online ISSN: 1530-7964.

[14] Baley C, Gomina M, Breard J, Bourmaud A, Davies P. Variability of mechanical properties of flax fibres for composite reinforcement. A review. Ind Crop Prod 2020;145:111984. http://dx.doi.org/10.1016/j.indcrop.2019.111984.

[15] Haag K, Padovani J, Fita S, Trouvé J-P, Pineau C, Hawkins S, et al. Influence of flax fibre variety and year-to-year variability on composite properties. Ind Crop Prod 2017;98:1–9. http://dx.doi.org/10.1016/j.indcrop.2016.12.028.

[16] Zwawi M. A review on natural fiber bio-composites, surface modifications and applications. Molecules 2021;26(2):404. http://dx.doi.org/10.3390/molecules26020404.

[17] Neto J, Queiroz H, Aguiar R, Lima R, Cavalcanti D, Banea M. A review of recent advances in hybrid natural fiber reinforced polymer composites. J Renew Mater 2021;10(3):561–89. http://dx.doi.org/10.32604/jrm.2022.017434, Online ISSN: 2164-6341.

[18] Flynn J, Amiri A, Ulven C. Hybridized carbon and flax fiber composites for tailored performance. Mater Des 2016;102:21–9. http://dx.doi.org/10.1016/j.matdes.2016.03.164.

[19] Dhakal HN, Zhang ZY, Guthrie R, MacMullen J, Bennett N. Development of flax/carbon fibre hybrid composites for enhanced properties. Carbohydr Polymers 2013;96(1):1–8. http://dx.doi.org/10.1016/j.carbpol.2013.03.074.

[20] Zhu J, Zhu H, Njuguna J, Abhyankar H. Recent development of flax fibres and their reinforced composites based on different polymeric matrices. Materials 2013;6(11):5171–98. http://dx.doi.org/10.3390/ma6115171.

[21] Dhaliwal GS, Dueck SM, Newaz GM. Experimental and numerical characterization of mechanical properties of hemp fiber reinforced composites using multiscale analysis approach. SN Appl Sci 2019;1(11):1361. http://dx.doi.org/10.1007/s42452-019-1383-6.

[22] Del Borrello M, Mele M, Campana G, Secchi M. Manufacturing and characterization of hemp-reinforced epoxy composites. Polym Compos 2020;41(6):2316–29. http://dx.doi.org/10.1002/pc.25540, Online ISSN: 1548-0569.

[23] Baysal A, Yayla P, Turkmen HS, Karaca Ugural B. Mechanical characterization of hybrid biocomposites reinforced with nonwoven hemp and unidirectional flax fibers. Polym Compos 2023;44(6):3555–66. http://dx.doi.org/10.1002/pc.27344, Online ISSN: 1548-0569.

[24] Del Bianco G, Giammaria V, Boria S, Fiumarella D, Ciardiello R, Scattina A, et al. Flax and hemp composites: Mechanical characterization and numerical modeling. Proc Inst Mech Eng C 2023;09544062231182036. http://dx.doi.org/10.1177/09544062231182036, Online ISSN: 2041-2983.

[25] Ismail SO, Akpan E, Dhakal HN. Review on natural plant fibres and their hybrid composites for structural applications: Recent trends and future perspectives. Composites C 2022;9:100322. http://dx.doi.org/10.1016/j.jcomc.2022.100322.

[26] Barouni A, Lupton C, Jiang C, Saifullah A, Giasin K, Zhang Z, et al. Investigation into the fatigue properties of flax fibre epoxy composites and hybrid composites based on flax and glass fibres. Compos Struct 2022;281:115046. http://dx.doi.org/10.1016/j.compstruct.2021.115046.

[27] Giammaria V, Del Bianco G, Raponi E, Fiumarella D, Ciardiello R, Boria S, et al. Material parameter optimization of flax/epoxy composite laminates under low-velocity impact. Compos Struct 2023;321:117303. http://dx.doi.org/10.1016/j.compstruct.2023.117303.

[28] Capretti M, Giammaria V, Santulli C, Boria S, Del Bianco G. Use of bio-epoxies and their effect on the performance of polymer composites: A critical review. Polymers 2023;15(24):4733. http://dx.doi.org/10.3390/polym15244733.

[29] Murariu M, Dubois P. PLA composites: From production to properties. Adv Drug Deliv Rev 2016;107:17–46. http://dx.doi.org/10.1016/j.addr.2016.04.003.

[30] Yan L, Chouw N, Jayaraman K. Flax fibre and its composites – A review. Composites B 2014;56:296–317. http://dx.doi.org/10.1016/j.compositesb.2013.08.014.

[31] Safri SNA, Sultan MTH, Jawaid M, Jayakrishna K. Impact behaviour of hybrid composites for structural applications: A review. Composites B 2018;133:112–21. http://dx.doi.org/10.1016/j.compositesb.2017.09.008.

[32] Bensadoun F, Depuydt D, Baets J, Verpoest I, Van Vuure A. Low velocity impact properties of flax composites. Compos Struct 2017;176:933–44. http://dx.doi.org/10.1016/j.compstruct.2017.05.005.

[33] Petrucci R, Santulli C, Puglia D, Nisini E, Sarasini F, Tirillò J, et al. Impact and post-impact damage characterisation of hybrid composite laminates based on basalt fibres in combination with flax, hemp and glass fibres manufactured by vacuum infusion. Composites B 2015;69:507–15. http://dx.doi.org/10.1016/j.compositesb.2014.10.031.

[34] Ahmed S, Ulven CA. Dynamic in-situ observation on the failure mechanism of flax fiber through scanning electron microscopy. Fibers 2018;6(1):17. http://dx.doi.org/10.3390/fib6010017.

[35] Obradovic J, Boria S, Belingardi G. Lightweight design and crash analysis of composite frontal impact energy absorbing structures. Compos Struct 2012;94(2):423–30. http://dx.doi.org/10.1016/j.compstruct.2011.08.005.

[36] LS-DYNA Keyword User's Manual, Vol II, Material Models, R13, Livermore Software Technology. 2021, URL: https://www.dynasupport.com/manuals/ls-dyna-manuals/ls-dyna_manual_volume_ii_r13.pdf.

[37] Rabiee A, Ghasemnejad H. Finite element modelling approach for progressive crushing of composite tubular absorbers in LS-DYNA: Review and findings. J Compos Sci 2022;6(1):11. http://dx.doi.org/10.3390/jcs6010011.